Journal of Magnetic Resonance 209 (2011) 352–358

Contents lists available at ScienceDirect

Journal of Magnetic Resonance

journal homepage: www.elsevier.com/locate/jmr

Communication

Compressed sensing and the reconstruction of ultrafast 2D NMR data: Principles and biomolecular applications

Yoav Shrot, Lucio Frydman *

Department of Chemical Physics, The Weizmann Institute of Science, Rehovot 76100, Israel

ARTICLE INFO

Article history:
Received 13 November 2010
Revised 11 January 2011
Available online 21 January 2011

Keywords:
Ultrafast 2D NMR
Non-linear reconstruction
Compressed sensing
Biomolecular spectroscopy

ABSTRACT

A topic of active investigation in 2D NMR relates to the minimum number of scans required for acquiring this kind of spectra, particularly when these are dictated by sampling rather than by sensitivity considerations. Reductions in this minimum number of scans have been achieved by departing from the regular sampling used to monitor the indirect domain, and relying instead on non-uniform sampling and iterative reconstruction algorithms. Alternatively, so-called "ultrafast" methods can compress the minimum number of scans involved in 2D NMR all the way to a minimum number of one, by spatially encoding the indirect domain information and subsequently recovering it via oscillating field gradients. Given ultrafast NMR's simultaneous recording of the indirect- and direct-domain data, this experiment couples the spectral constraints of these orthogonal domains – often calling for the use of strong acquisition gradients and large filter widths to fulfill the desired bandwidth and resolution demands along all spectral dimensions. This study discusses a way to alleviate these demands, and thereby enhance the method's performance and applicability, by combining spatial encoding with iterative reconstruction approaches. Examples of these new principles are given based on the compressed-sensed reconstruction of biomolecular 2D HSQC ultrafast NMR data, an approach that we show enables a decrease of the gradient strengths demanded in this type of experiments by up to 80%.

1. Introduction

Two-dimensional nuclear magnetic resonance (2D NMR) provides valuable information for resolving and identifying the nature of chemical sites in a variety of chemical and biochemical systems. The data acquisition paradigm for 2D spectroscopy originates from the suggestion by Jeener, Ernst and their coworkers [1,2], to record the signal emitted by a spin system as a function of two independent time variables: t_2, a run-time variable associated with a direct physical measurement; and t_1, a parametric delay that is systematically incremented throughout a series of independent experiments. Spectral information can be retrieved from this 2D time-domain matrix by a fast Fourier Transformation (FT), best implemented when using a uniform sampling of the time variables. A restricting factor, however, is imposed by this choice of sampling: as each of the parametric increments Δt_1 required to suitably map the indirect-domain is associated with an independent scan, the minimum number of experiments that will be needed, N_1, is determined by the indirect-domain spectral width ($SW_1 = 1/\Delta t_1$) and by the associated spectral resolution ($\Delta\nu_1 = 1/t_1^{\max} = 1/N_1\Delta t_1$), according to $N_1 = SW_1/\Delta\nu_1$. This is a restriction arising from the demands posed by the actual form of sampling the data, rather than from signal-to-noise ratio (SNR) considerations. Therefore, various strategies have been suggested to bypass it, and reduce the minimum number N_1 of required scans. Main routes proposed for this relies on exploiting spectral information available from *a priori* 1D NMR measurements, and use this for either a selective addressing of the spectral peaks of interest along the ν_1 indirect domain [3,4], or for "unfolding" these from aliased spectral windows upon post-processing [5]. Another group of methods aims to reconstruct the spectra of interest by departing from traditional Nyquist time-domain sampling criteria altogether, for instance utilizing reduced-dimensionality measurements [6–8] or non-uniformly sampling of the indirect domains whose results are processed using non-fast-FT algorithms [9–13]. Included among the latter algorithms are maximum entropy, maximum likelihood, frequency decomposition, and a number of other algorithms that rely on some form of regularization to stabilize what could otherwise become an ill-conditioned inversion problem. All these approaches are based on the commonly fulfilled premise that sensitivity is sufficiently high, and that the number of spectral lines in the indirect domain is considerably smaller than the number of scans required by the FT paradigm.

As an alternative to these methods, recent years have witnessed the emergence of "ultrafast" approaches [14–16], capable of reducing the total number of scans required in 2D spectroscopy from a different perspective. These approaches rely on concepts derived

* Corresponding author. Fax: +972 8 9344123.
E-mail addresses: yoav.shrot@weizmann.ac.il (Y. Shrot), lucio.frydman@weizmann.ac.il (L. Frydman).

1090-7807/$ - see front matter © 2011 Elsevier Inc. All rights reserved.
doi:10.1016/j.jmr.2011.01.017

from NMR imaging, to parallelize all N_1 experiments involved in a 2D NMR measurement so as to complete it in a single scan. To do so ultrafast 2D NMR endows each voxel within the sample with an indirect domain evolution time that is proportional to its position z, i.e. $t_1(z) = C \cdot z$ with C a spatio-temporal constant under the experimentalist's control. The linearly distributed evolution time provides the transverse magnetization of nuclei with a chemical shift of Ω_1, with a phase of $\phi(z) = C \cdot \Omega_1 \cdot z$. When summed over the entire sample the resulting winding of magnetizations will generate no signal; yet in the presence of a field gradient possessing an appropriate orientation and magnitude, this helical magnetization pattern can be unwound, and bring all the spins into phase to form a macroscopic echo. Defining for this latter gradient a wavenumber $k(t) \equiv \int_0^t \gamma_a G_a(\tau) d\tau$, these echoes will be formed when $k = -C\Omega_1$ establishing, in a one-to-one fashion, a correspondence between the k-variable and the v_1 indirect-domain frequency axis. To extract the full information contained in a 2D experiment, the ultrafast strategy thus applies a rapid oscillation of the acquisition gradient G_a; this oscillation unravels the indirect domain information multiple times, and monitors it as it evolves as a function of the direct-domain time t_2. A typical acquisition trajectory generated by a square-wave oscillation of this decoding gradient in the k/v_1–t_2 plane, is depicted in Fig. 1A. This Figure evidences how, when the positive and negative gradients used to unravel the spatially encoded magnetization windings have equal magnitudes, every k/v_1-echo – and therefore every "peak" in the indirect-domain spectrum – is sampled twice during each oscillation period. Moreover, if considering just the positive or negative gradient applications, every k/v_1-echo is sampled at exactly $2 \cdot T_a$ time intervals along t_2. Either one of these "positive" or "negative" sets can therefore be independently processed by fast FT, and subsequently co-added for improving the overall SNR. (Alternatively, the may be jointly processed in a single transformation leading also to improved SNR by the interlaced FT [17].) Regardless of

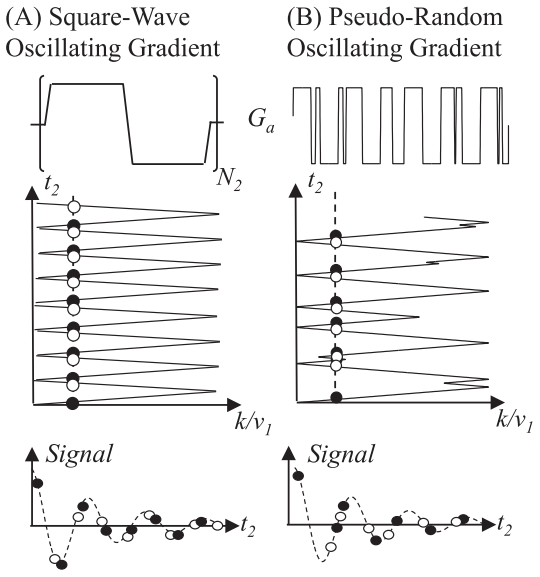

Fig. 1. Strategies explored in this work for ultrafast 2D NMR acquisitions. (A) Traditional scheme based on a constant square-wave modulation of the acquisition gradient G_a. (B) Pseudo-random approach assayed in this study for the sake of an iterative v_2 reconstruction. The upper and middle panels display the G_a waveforms and their corresponding k/v_1–t_2 trajectories. The bottom row considers a cross section of these trajectories for a given k/v_1-value (dashed line), and shows the sampled FID points with black and white dots denoting data recorded during positive and negative gradient, respectively. Unlike the regular sampling provided by the square-wave modulation in (A), the random sporadic sign-changes in waveform (B) provide a sampling pattern that is suitable for an iterative reconstruction that is not necessarily bound by Nyquist criteria.

which route is implemented for doing such FTs, the direct-domains of the resulting spectra will be characterized by similar relations: in both cases their spectral widths SW_2 will inversely proportional to T_a, and their corresponding resolutions Δv_2 be given by the extent of the sampling along the direct-domain time axis, $t_2^{\max}$. As for the indirect domain, the extent of its spectral 2 characterization will be given by the encoding characteristics and by the range of k/v_1-space that has been scanned. In particular, for a given indirect-domain target SW_1, the amplitude of the G_a acquisition gradient will become inversely proportional to T_a – that is, proportional to SW_2 [16]. Thus, the fact that this method enables the acquisition of arbitrary 2D spectra within a single scan, also means that spatial encoding will tie together demands on the spectral parameters of the various sampled axes according to

$$\frac{SW_1 SW_2}{\Delta v_1} \sim \gamma_a G_a L, \tag{1}$$

where as mentioned Δv_1 and SW_1 are the indirect-domain spectral resolution and bandwidth, SW_2 is the direct-domain spectral width, G_a the gradient amplitude (assumed of constant magnitude during the acquisition), and L is the sample's length. Notice that since L is a constant and the maximal gradient strength that can be imparted on G_a may be limited, a tradeoff among the characteristics of the direct- and indirect-domains may end up being unavoidable. Moreover, even if strong enough gradients are available to fulfill all spectral width demands, increasing G_a's amplitude requires a concomitant opening of the receiver's bandwidth, which in turn increases the noise level in proportion to the square-root of Eq. (1)'s right-hand side.

It follows from these arguments that reducing the maximum gradient's amplitude is always desirable in ultrafast 2D NMR – whether to ease the hardware demands or to improve the method's SNR. Several approaches have been put forward for this purpose, in all cases using *a priori* information about the indirect-domain to optimize the encoding of its interactions [18–20]. Recently developed spatial/spectral manipulations, for example, uniformly distribute the echoes expected to arise from different chemical sites along the k/v_1-axis. This in turn transforms Eq. (1) into

$$n_1 \cdot SW_2 \sim \gamma_a G_a L, \tag{2}$$

where n_1 is the number of peaks known to arise along the indirect domain. Dealing with a sparse indirect-domain spectrum can therefore reduce considerably the demands on G_a, while making no compromises on the indirect-domain's resolution or bandwidth. Notice, however, that this method still relies on reading the indirect-domain echoes using an acquisition whose overall scheme is identical to that of ultrafast 2D NMR, and which is bound by the same fast FT considerations. Therefore, although the k/v_1-range can be considerably reduced, no departures from Shannon-Nyquist sampling criteria are involved. Still, the current work demonstrates that the coupling of non-linear sampling and of suitable data processing methods can be harnessed for ultrafast methodologies, provided that they focus on alleviating the Nyquist demands of the *direct* domain. In particular this Communication demonstrates that by departing from the usual, square-wave G_a modulation characteristic of ultrafast acquisitions, and by incorporating iterative algorithms like compressed sensing, it is possible to lift stringent relations of the kind embodied by Eqs. (1) and (2), and enable the acquisition of improved ultrafast 2D NMR spectra.

2. Numerical methodology

The methods used as basis for this research, share a common approach with those normally used when iterative algorithms are employed to speed up other kinds of NMR or MRI nD data acquisitions [9–13]. Like those counterparts, we will also rely on a

non-uniform sampling pattern and a numerical algorithm that frees the spectrum retrieval process from the constraints posed by the fast FT. In conventional nD NMR spectroscopy/imaging this enables the reconstruction of frequency-domain data based on the acquisition of considerably fewer scans than those demanded by the Shannon criterion. In ultrafast NMR/MRI spectroscopy, however, where the number of scans has already been decreased to a minimal value, speed-up goals are no longer relevant. Moreover, given the absence of FT along the spatially encoded domain, extracting the indirect-domain spectrum by numerical means is also not pertinent. Still, the additional flexibility provided by non-FT methods can be harnessed for another purpose: reducing the amplitude of the G_a decoding gradients, and thereby alleviate the technical and sensitivity problems that were alluded to earlier. This will in turn imply applying iterative reconstruction methods along t_2-axis over which these gradients operate. Such procedures have to our knowledge not been applied before to dealing with the direct domain of 2D NMR, as its information comes here nearly "for free" in both time and sensitivity. The coupling of the G_a and SW_2 put forward by Eq. (1), however, lead us to consider the consequence of using non-FT methods along ultrafast NMR's direct-domain.

One of the essential ingredients required for departing from the criteria imposed by fast FT processing, is to abandon the use of equi-spaced data sampling patterns: only in such a way can aliasing be avoided, and genuine frequencies be extracted from a time-domain response over a range that is no longer bound by the Nyquist limit [26]. It follows that the gradient waveform normally used in ultrafast NMR (Fig. 1A) will not serve this purpose: by providing for each k/v_1 echo a sampling pattern that is uniform along t_2, this periodic G_a square-wave will not deliver a randomized array of time-domain points like the one required by non-FT processing. A non-uniform t_2 pattern, however, can easily be introduced by imposing onto the gradient waveform a pseudo-random sign alteration. This alternation should not be entirely random, as the k/v_1-axis also needs to probe a predefined indirect-domain range SW_1 of frequencies. Changes imparted on G_a should therefore be tailored so as to fulfill a suitable coverage of a given targeted indirect-domain spectral region. Fig. 1B illustrates one route for achieving this, with a potential gradient waveform and its resulting trajectory in the k/v_1–t_2 space. A proper rearrangement of points sampled during the resulting FID will provide, for each coordinate along the k/v_1-axis, an individual set of randomly distributed points along t_2 (Fig. 1B, bottom). Iterative algorithms can then be used for each coordinate along k/v_1, to reconstruct the associated 1D spectrum arising along the direct-domain, and from there the full 2D distribution being sought.

The consequences of following this approach were here explored with the aid of a compressed sensing reconstruction of the expected 2D spectra [13,21–25] – even if other methods [9–12,27] could also have been used. Compressed sensing relies on a number of basic assumptions. One is that the spectral information being sought is sparse; i.e., that most of the frequency coordinates within the targeted range do not contain any information. This premise may seldom be fulfilled for the 1D direct-domain NMR spectrum as a whole, but will often be valid when considering that our problem will only deal with rows of the full 2D interferogram, whereby the data to be reconstructed has already been separated into the numerous k/v_1 making up the whole 2D distribution. Each of the 1D direct-domain spectra being sought can then, with high probability, be reconstructed by fitting its corresponding FID to a function S, fulfilling the minimization of the so-called ℓ_1-norm

$$\min_S \|S\|_1 \quad \text{under FID}(\{t_p\}) = \underline{\underline{A}} \cdot S, \tag{3}$$

where $\ell_1(x) \equiv \|x\|_1 \equiv \sum_i |x_i|$. The $\underline{\underline{A}}$ operator in Eq. (3) represents the Fourier transform of the spectrum S, which takes into account that its corresponding FID was sampled at a series of arbitrary direct-domain times $\{t_p\}$. Several methods have been proposed to solve this numerical fitting problem; this study implements one of the simplest forms based on an iterative soft thresholding [13,23]. In order to estimate the spectral distribution S this algorithm makes a series of iterations, preserving in each of these only those spectral components that are clearly distinguishable from potential numerical or thermal noises. The algorithm then adds these "peaks" to a reconstructed spectrum, and filters out the residual according to a thresholding operator defined by

$$(\delta_\lambda(y))_q = e^{i\cdot\angle y_q}\left(|y_q| - \lambda\right)_+. \tag{4}$$

This operation returns zero if the magnitude of the residual's spectral input for a particular y_q value is below a threshold λ, and reduces its amplitude otherwise while keeping the input's original phase. The expected FID generated by the reconstructed spectrum is calculated and subtracted from the initial FID; the result is then used as input for a subsequent iteration. The pseudocode of the algorithm used in this study to recover in this manner a full 2D spatially encoded spectrum, is presented in Table 1.

Table 1
Pseudocode for the iterative soft thresholding processing of ultrafast 2D NMR data.

Input:
G(t) – gradient waveform ($N \times 1$); FID ($N \times 1$); k/v_1 – axis grid ($n \times 1$); v_2 – the direct domain frequency vector ($1 \times m$), ε, MaxIter – maximal number of iterations
Output:
$S(k/v_1, v_2)$ – 2D spectrum matrix (n-by-m):
Preliminary calculations:
$k(t)$ – wavenumber as a function of acquisition
$t_2(k)$ – n vectors containing the t_2 points at each wavenumber k
$\underline{\underline{A}}_k = \exp(i \cdot 2\pi \cdot (t_2(k))^T v_2)$ – n complex matrices
Initialization:
Residual vectors $r_0(k) = \text{FID}(k, t_2)$
Correlation vectors $c_0(k) = \underline{\underline{A}}_k^\dagger r_0(k)$
Global threshold value $\lambda_0 = \mu \cdot \max\{|c_0(k)|\}$
Solution $S_0 = 0$ of size $n \times m$
while ($p <$ MaxIter) and ($||r_p||_2 \geqslant \varepsilon\ ||\text{FID}||_2$):
Update solution $S_{p+1}(k) = S_p(k) + \delta_{\lambda_p}(c_p(k))$
Calculate residual $r_{p+1}(k) = FID(k) - \underline{\underline{A}}_k S_{p+1}(k)$
Calculate correlation $c_{p+1}(k) = \underline{\underline{A}}_k^\dagger r_{p+1}(k)$
Update threshold value $\lambda_{p+1} = \mu \cdot \max\{|c_{p+1}(k)|\}$
end while
Post-processing: Inverse FT for $S(k/v_1, v_2)$ along the direct domain; exponential, Gaussian or lorentzian filtering; FT for $S(k/v_1, v_2)$ along the direct domain.

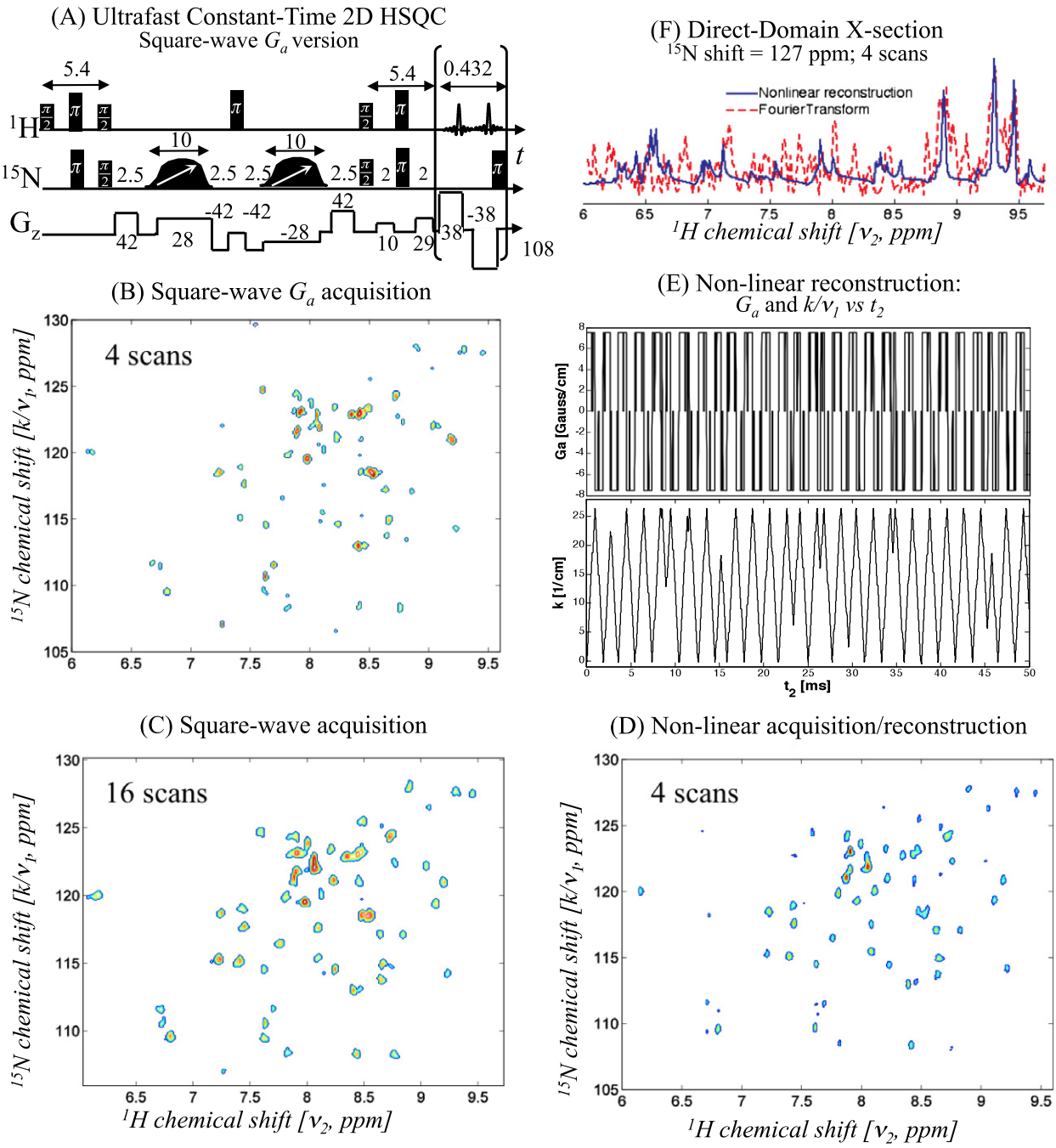

Fig. 2. (A) Scheme of the constant-time, spatially-encoded HSQC sequence assayed. All timing and gradient strength values used are indicated in units of ms and G/cm, respectively; water suppression was implemented by strong purge gradient pulses; acquisition dwell times were set to 2 μs; and following each gradient cycle a hard 66 μs π pulse was used for ^{15}N decoupling. In order to achieve a high resolution along the indirect domain the experiments used a relatively long 20 ms encoding period. (B) Purely-absorptive 2D spectrum obtained on an aqueous Ubiquitin solution using the conventional $\pm G_a$ square-wave acquisition gradient, after signal averaging four scans and displayed at a contour level of 50%. Only the positive gradient data set was processed by zero-filling, exponential apodization with a decay time of 30 ms along t_2, and fast FT. Given the strong acquisition gradients employed, the receiver's bandwidth was correspondingly set to $\gamma_a G_a L$ = 290 kHz (L = 1.8 cm). (C) Idem as (B) but after signal averaging sixteen scans, and plotted at a 40% contour level. (D) Idem as (B), but upon subjecting the data to an iterative reconstruction. The gradient waveform used in this acquisition is shown in panel (E), which also shows the non-periodic trajectory resulting in the k/ν_1–t_2 plane. The actual $G_a(t_2)$ waveform incorporated rise/fall times of 16 μs, and a zero-gradient period of 66 μs every 634 μs for performing the ^{15}N-decoupling via hard π pulses. By lifting the stringent sampling demands of the fast FT, the overall $|G_a|$ strength reduced to 7.5 G/cm. The ensuing reduction in receiver's bandwidth enabled the reconstruction of a high-quality spectrum using only four scans: data in (D) are shown at a 25% contour level. A more explicit comparison between the spectral SNRs arising from the two transforms is illustrated by the cross-sections (F), extracted at the indicated indirect-domain shift from the corresponding four-scan experiments. The reconstruction leading to this spectrum involved an iterative fit according to Table 1 using μ = 0.9, on a spectral region of ±1.2 kHz with a resolution of 6 Hz. These fits were terminated after 250 iterations (increasing the number of iterations did not induce appreciable change in the 2D spectra) and following their implementation the resulting vectors were inversed-FT along the direct domain, weighted with a 30 ms exponential decay, and forward-FT to provide the final spectrum. On a dual core, 2.2 GHz CPU, the overall time required to process such data set took under 60 s.

Another requirement for achieving a successful compressed sensing reconstruction, is to secure a sufficient number of t_2 points for every k/ν_1 value. Indeed, a proper characterization of the ν_2 spectrum will only arise if this set of points is substantially larger than the number of inequivalent peaks arising along the direct-domain for every k/ν_1 coordinate. Noting that different k/ν_1 points

cannot be measured simultaneously, that the same G_a physical gradient needs to be used to reach sequentially the different k/v_1 coordinates, and that the strength of the G_a used is finite, it follows that an excessive focusing on one region of the k/v_1-axis will degrade the performance of the sampling imparted at some other k/v_1 region. This constraint, taken in unison with the presence of a T_2 relaxation that puts a limit to the maximal acquisition time that can be used, implies that in order to exploit this kind of processing strategy one should choose the continuous gradient waveform that will be used, with an average cycle period that is uniformly longer for every sampled k/v_1 coordinates. To implement this we relied on relatively small random factors imparting these variations G_a, which added or subtracted from the normal square-wave modulation period $2T_a$. The chance to switch signs at any point along the gradient waveforms computed in this study, was assumed to be only in the range of 0.1%–0.2%. This lead to the kind of waveforms and k–t_2 space trajectories illustrated in Fig. 1B. Naturally, the sparser the spectrum under investigation is, the more flexible one can be in this choice of parameters and the larger a randomness factor can be used. This in turn leads to spectra that can be retrieved using weaker gradients than in the conventional FT-based ultrafast 2D NMR approach, an advantage whose ensuing qualities are illustrated by the experimental results below.

3. Experimental

In order to demonstrate the potential advantages of compressed sensing reconstruction in ultrafast 2D NMR, a ≈2 mM sample of ^{15}N-enriched Ubiquitin dissolved in a 90%/10% H_2O/D_2O buffer was analyzed. Constant-time spatially-encoded 2D HSQC NMR experiments were recorded on such sample [16,28], using a 14 T magnet and a Varian VNMRS© spectrometer equipped with a triple channel probe possessing a single, linear z-gradient. Square-wave acquisition gradients were used for performing the normal ultrafast 2D NMR experiments and taken as reference; custom waveforms were generated and used for the iterative spectral reconstruction experiments. All of these waveforms, their ancillary RF pulses and the data processing algorithms, were written using customized Matlab programs that are available upon request.

4. Results

Two sets of compressed-sensing HSQC NMR experiments were carried out on the targeted 8.5 kDalton protein, aimed at demonstrating the sensitivity advantages that could result from exploiting this iterative processing. These sets differed in the duration of the

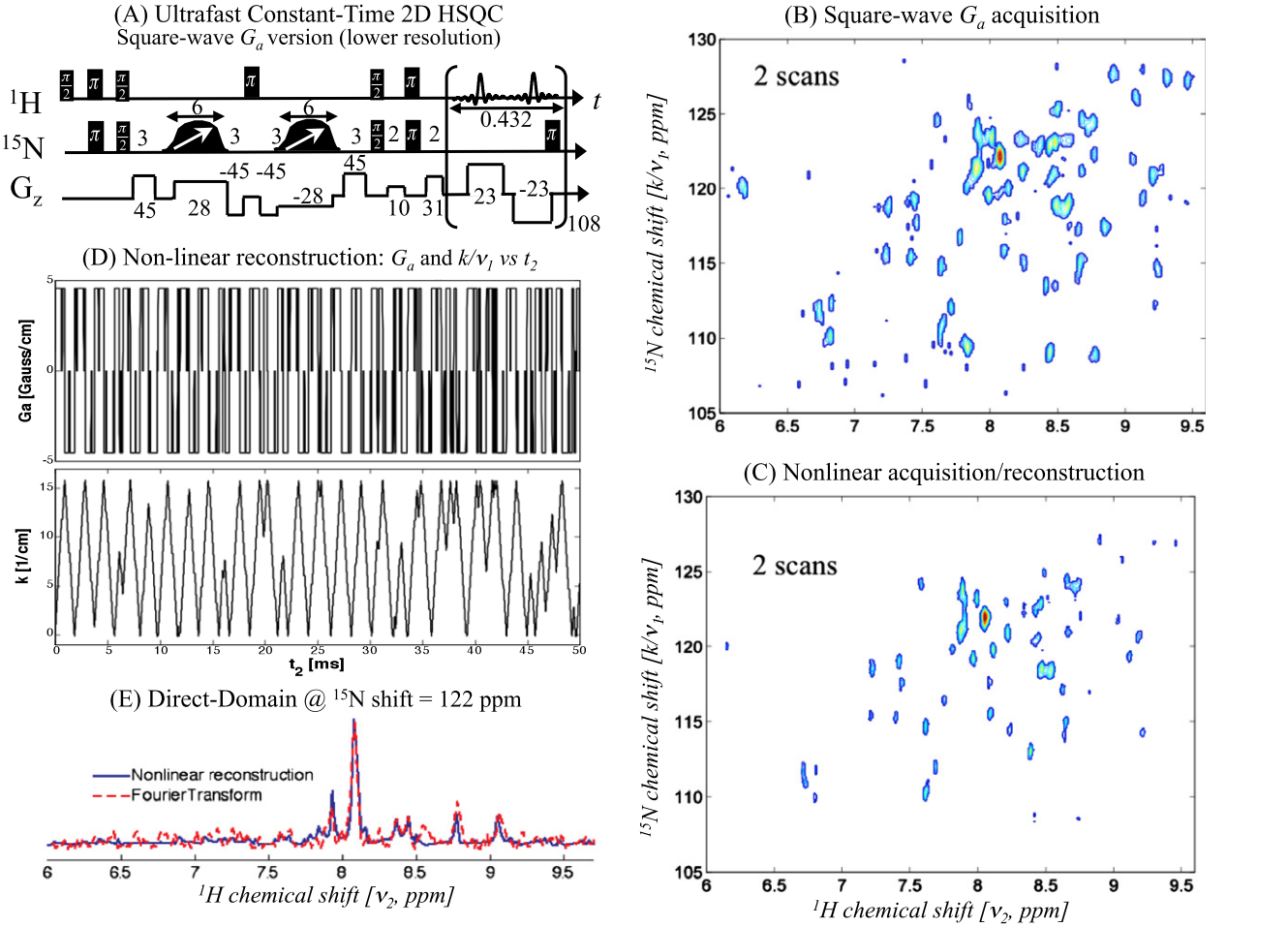

Fig. 3. Analog results as shown in Fig. 2, but for spatially-encoded 2D HSQC acquisitions involving a lower v_1-resolution, and hence a higher SNR. (A) Schematic pulse sequence used. (B) 2D purely absorptive spectrum obtained using a conventional G_a = ±23 G/cm square-wave modulation (same as in Fig. 2A but with a 40% smaller gradient). The reduced gradient allowed us to use a narrower receiver bandwidth, and hence acquire a spectrum in only two scans. Processing was as for Fig. 2B, and the spectrum is displayed at a 20% contour level. (C) Purely-absorptive HSQC spectrum obtained using a non-periodic sampling and a iterative reconstruction approach, enabling acquisitions with $|G_a| \leqslant 4.5$ G/cm and leading to a ×3 SNR improvement. These two-scan data are shown at a 20% contour level, and their processing involved similar characteristics as for Fig. 2D. (D) Non-periodic gradient waveform used in the latter acquisition, and corresponding k/v_1–t_2 trajectory. (E) Cross-sections arising at a ^{15}N shift of 122 ppm, illustrating the corresponding SNRs.

maximum encoding period t_1^{max} utilized: the longer this encoding is the higher the resulting resolution of the indirect spectral domain, but a larger G_a gradient is then needed (*cf.* Eq. (1)), and thereby a lower SNR will result. Fig. 2 illustrates how this penalty can be bypassed by the new methods hereby discussed, utilizing as test case a sequence with a relatively long encoding period (20 ms, Fig. 2A). Given this choice of t_1^{max} and the spectral bandwidths to be targeted, a relatively large $|G_a| \approx 38$ G/cm square-wave gradient had to be used for fulfilling the sampling criteria of normal ultrafast NMR acquisitions. Most peaks are still discernable in the 2D plot when four scans are used (Fig. 2B), but spectra only exhibits good SNR after averaging signals over 16 scans (Fig. 2C). By comparison, Fig. 2D displays the results obtained upon using only four scans, but with a pseudo-random alternating gradient. A significantly higher SNR is visible upon subjecting these data to a compressed-sensing spectral reconstruction, and comparing it against its conventional counterpart. This reflects the fact that, as it is no longer necessary to rely on a constrained T_a period to sample the full wavenumber range, a fivefold weaker $|G_a|$ value can be used without compromising the indirect-domain's SW_1 (see the corresponding waveforms used in this experiment in Fig. 2E). These remarkably smaller amplitudes enable one in turn to decrease the receiver's bandwidth by a similar factor, and arrive at ca. $\times 2$ improvements in SNR.

It follows from Eq. (1) that sensitivity can also be improved by demanding a smaller resolution along the indirect-domain; i.e., by reducing the t_1^{max}. The acquisition gradient can then be decreased, and good SNR obtained for the kind of targeted sample even if using a conventional square-wave acquisition gradient. These features can be appreciated by comparing the data in Fig. 2 with the panels Fig. 3A and B, which show how a reduction of t_1^{max} to 12 ms allows one to reduce $|G_a|$ to 23 G/cm, and thereby get good spectral SNR using the usual ultrafast acquisition mode in only two scans. Yet again, also under such conditions, advantage can be taken from the iterative reconstruction schemes that lead to an even better SNR (Fig. 3C). This once again reflects the nearly fivefold reduction in the $|G_a|$ amplitude (Fig. 3D), that are made possible by combining the use of non-linear data sampling and iterative reconstructions.

5. Discussion and conclusions

The examples shown in Figs. 2 and 3 demonstrate that, even when dealing with moderately complex spectra, sensitivity advantages can be obtained from iterative reconstruction schemes. By allowing one to non-uniformly sample the direct domain, these enable the use of weaker gradient amplitudes than would be normal in ultrafast 2D NMR, bringing about ensuing reductions in noise. This does not mean, however, that one can always benefit from relying on iterative reconstruction algorithms in this kind of experiments. One issue limiting the applicability of these schemes concerns the sparsity criteria, which may not be applicable along every k/v_1 coordinate of the sampled interferogram. Fulfilling this demand may require, for more complex biomolecules than Ubiquitin, the introduction of additional spectral dimensionalities. Another concern arises from the higher sensitivities that iterative reconstruction protocols like the one here assayed, may have to the level of noise characterizing the sampled data – particularly concerning their numerical stability. Indeed, whereas the fast FT is a stable procedure where output and input noise are always linearly dependent on one another, the faithfulness of non-linear numerical schemes will depend in a complex way on the level of the input noise affecting the fitted FID. Therefore, although iterative processing could in principle always allow one to reduce the acquisition gradient, the SNR will, in general, vary in a complex way with the receiver bandwidth and/or with the number of signal averages. This noise sensitivity was also found to be dependent on the validity of the sparseness assumption: the denser the spectrum to be reconstructed is, the more sensitive it becomes to the input noise. This in turn may end up resulting in counter-intuitive effects. For instance: whereas demanding low resolution along the indirect-domain allows one to weaken the G_a gradient, this loss in resolution will also broaden the v_1 lines, and endow (on average) every k-coordinate with an effectively denser direct-domain spectrum. This in turn, may increase the numerical noise associated to the reconstruction – rather than decrease it, as could have been expected from purely bandwidth-related arguments. On the other hand, the new flexibility introduced by the iterative processing methods can always be exploited without compromises, to enable the scanning of a considerably larger k/v_1-range, corresponding to an enlargement of the indirect-domain spectral width SW_1. Compressed sensing methods could also be combined with spatial encoding paradigms other than those involved in the usual ultrafast 2D NMR experiment, for instance with the above-mentioned techniques that optimize the positioning of the peaks in the indirect domain [18–20], and thereby extend even further the applicability of ultrafast spectroscopy to a wider range of systems and setups. Beyond these purely 2D spectroscopy applications, compressed sensing continues to be extensively and very successfully used in rapid MRI applications [24,25]. The modifications that were here described could also make it useful in other kinds of applications – including mixed spectroscopic/imaging ones. These subjects will be further developed in upcoming publications.

Acknowledgments

This research was supported by the Israel Science Foundation (ISF 447/09), the European Commission (BioNMR, Project No. 261863), ERC Advanced Grant #246754, a Helen and Kimmel Award for Innovative Investigation, and the generosity of the Perlman Family Foundation.

References

[1] J. Jeener, Lecture Presented at Ampere International Summer School II, Basko Polje, Yugoslavia, 1971.
[2] R.R. Ernst, G. Bodenhausen, A. Wokaun, Principles of Nuclear Magnetic Resonance in One and Two Dimensions, Oxford, 1987.
[3] E. Kupce, R. Freeman, Two-dimensional hadamard spectroscopy, J. Magn. Reson. 162 (2003) 300–310.
[4] E. Kupce, T. Nishida, R. Freeman, Hadamard NMR spectroscopy, Prog. Nucl. Magn. Reson. Spectrosc. 42 (2003) 95.
[5] D. Jeannerat, High resolution in the indirectly detected dimension exploiting the processing of folded spectra, Magn. Reson. Chem. 38 (2000) 415.
[6] S. Kim, T. Szyperski, GFT NMR, a new approach to rapidly obtain precise high-dimensional NMR spectral information, J. Am. Chem. Soc. 125 (2003) 1385.
[7] E. Kupce, R. Freeman, Projection-reconstruction technique for speeding up multidimensional NMR spectroscopy, J. Am. Chem. Soc. 126 (2004) 6429.
[8] S. Hiller, F. Fiorito, K. Wüthrich, G. Wider, Automated projection spectroscopy (APSY), Proc. Natl. Acad. Sci. USA 102 (2005) 10876.
[9] V.A. Mandelshtam, The multidimensional filter diagonalization method. I. Theory and numerical implementation, J. Magn. Reson. 144 (2000) 343.
[10] J.C. Hoch, A.S. Stern, Maximum entropy reconstruction, spectrum analysis and deconvolution in multidimensional nuclear magnetic resonance, Methods Enzymol. 338 (2001) 159.
[11] D. Marion, Fast acquisition of NMR spectra using Fourier transform of non-equispaced data, J. Biomol. NMR 32 (2005) 141–150.
[12] K. Kazimierczuk, W. Kozminski, I. Zhukov, Two-dimensional Fourier transform of arbitrarily sampled NMR data sets, J. Magn. Reson. 179 (2006) 323–328.
[13] I. Drori, Fast l1 minimization by iterative thresholding for multidimensional NMR spectroscopy. EURASIP. J. Adv. Signal. PR. (2007) 1.
[14] L. Frydman, T. Scherf, A. Lupulescu, The acquisition of multi-dimensional NMR spectra within a single scan, Proc. Natl. Acad. Sci. USA 99 (2002) 15859–15862.
[15] Y. Shrot, L. Frydman, Spatial encoding strategies for ultrafast multidimensional nuclear magnetic resonance, J. Chem. Phys. 128 (2008) 052209.
[16] M. Gal, L. Frydman, Ultrafast Multidimensional NMR: Principles and Practice of Single-scan Methods, in: G.A. Morris, J.W. Emsley (Eds.), Multidimensional NMR Methods for the Solution State, John Wiley & Sons Ltd, Chichester, UK, 2010, pp. 43–60.
[17] M. Mishkovsky, L. Frydman, Interlaced Fourier transformation of ultrafast 2D NMR data, J. Magn. Reson. 173 (2005) 344–350.

[18] P. Pelupessy, L. Duma, G. Bodenhausen, Improving resolution in single-scan 2D spectroscopy, J. Magn. Reson. 194 (2008) 169–174.
[19] A. Tal, B. Shapira, L. Frydman, Single-scan 2D hadamard NMR spectroscopy, Angew. Chem. 121 (2009) 2770.
[20] Y. Shrot, L. Frydman, Spatial/spectral encoding of the spin interactions in ultrafast multidimensional NMR, J. Chem. Phys. (131) (2009) #224512.
[21] D. Donoho, Compressed sensing, IEEE Trans. Inform. Theory 52 (2006) 1289.
[22] E.J. Candes, J. Romberg, T. Tao, Robust uncertainty principles: exact signal reconstruction from highly incomplete frequency information, IEEE Trans. Inform. Theory 52 (2006) 489.
[23] A.S. Stern, D. Donoho, J.C. Hoch, NMR data processing using iterative thresholding and minimum l1-norm reconstruction, J. Magn. Reson. 188 (2007) 295–300.
[24] M. Lustig, D. Donoho, J.M. Pauly, Sparse MRI: the application of compressed sensing for rapid MR imaging, Magn. Reson. Med. 58 (2007) 1182–1195.
[25] M. Lustig, D. Donoho, J.M. Santos, J.M. Pauly, Compressed sensing MRI, IEEE Signal Process. 25 (2008) 72–82.
[26] G.L. Bretthorst, Nonuniform sampling: bandwidth and aliasing, Concepts Magn. Reson. A 32 (2008) 417–435.
[27] K. Kazimierczuk, J. Stanek, A. Zawadzka, W. Kozminski, Random sampling in multidimensional NMR spectroscopy, Prog. NMR Spect. 57 (2010) 420–434.
[28] P. Pelupessy, Adiabatic single scan two-dimensional NMR spectrocopy, J. Am. Chem. Soc. 125 (2003) 12345–12350.